

**ac conductance in granular insulating Co-ZrO<sub>2</sub> thin films: A universal response**

Zorica Konstantinović, Montserrat García del Muro, Miroslavna Kovylyna, Xavier Batlle, and Amílcar Labarta  
*Departament de Física Fonamental and Institut de Nanociència i Nanotecnologia, Universitat de Barcelona, Martí i Franquès 1,  
 08028-Barcelona, Spain*

(Received 9 September 2008; published 20 March 2009)

The ac conductance in granular insulating Co-ZrO<sub>2</sub> thin films prepared by pulsed laser deposition is systematically studied as a function of the Co volume content  $x$ . An absorption phenomenon at low frequencies that mimics the *universal* response of disordered dielectric materials is observed in the range of metal content below the Co percolation threshold  $x_p \approx 0.35$  in the so-called dielectric regime. The temperature and frequency dependences of this absorption phenomenon are successfully analyzed in terms of random competing conduction channels between Co particles through thermally assisted tunneling and capacitive conductance. The ac conductance is well correlated with the nanostructure of the samples obtained by the transmission electron microscopy and perfectly matches the calculated ac response for a random resistor-capacitor network. We also show the occurrence of fractional power-law dependences on the frequency of the ac conductance taking place at very low frequencies as compared to the typical ranges at which dispersive behavior is observed in classical-disordered dielectric materials.

DOI: [10.1103/PhysRevB.79.094201](https://doi.org/10.1103/PhysRevB.79.094201)

PACS number(s): 61.82.Rx, 68.55.-a

**I. INTRODUCTION**

Granular materials comprise a very active research field due to their relevant properties and potential applications.<sup>1</sup> Granular materials are constituted by a random distribution of small particles embedded in an either metallic or insulating matrix. When particles are reduced to nanometer sizes, their properties differ considerably from the corresponding bulk counterpart, giving rise to new phenomena which result from finite-size, surface, and proximity effects, and interparticle interactions, leading to a variety of enhanced properties.<sup>2–12</sup> While dc transport properties of insulating granular thin films have been widely studied since 1970s,<sup>4,5,7–10</sup> much less attention has been paid to the ac response of these systems, for which many effects are not yet completely understood. In particular, we recently showed that the ac electrical properties of Co nanoparticles embedded into a dielectric ZrO<sub>2</sub> matrix display a complex low-frequency absorption phenomenon<sup>11,12</sup> in the dielectric regime below the percolation threshold for Co that mimics the so-called *universal response*<sup>13</sup> of disordered dielectric materials, which remains a topic of very active experimental and theoretical researches.<sup>14–17</sup> In particular, the ac conductivity and permittivity are characterized in disordered dielectric materials by the existence of a transition above a critical value of the angular frequency from a low-frequency dc plateau to a dispersive high-frequency region, where both the conductivity and the permittivity show an anomalous fractional power-law dependence on the angular frequency.<sup>13,17</sup> This dispersive behavior has been observed in a large variety of materials,<sup>14</sup> suggesting that the *universal response* is an intrinsic property associated with the geometry and actual characteristics of the conduction network rather than the specific mechanisms responsible for the conduction processes and the nature of the atoms constituting those materials. Some theoretical works have claimed the existence of a unique value of the fractional exponent for the conductivity around 0.7.<sup>17,18</sup> However, the large dispersion of values ob-

tained from experimental results and a recent work by Papanthassiou *et al.*<sup>19</sup> cast doubts on the universality of the fractional exponent.

While that *universal* ac response is thus common to disordered dielectrics, such as semiconductors, polymers, ion conducting glasses, and granular insulating thin films, the existence of disordered electrical paths appears to be the only common feature to all of those systems. In particular, the particle-size distribution observed in Co-ZrO<sub>2</sub>, which is intrinsic to any granular system, yields randomly competing thermally assisted tunneling through small particles and capacitive conductance channels among larger particles that are further apart.<sup>20</sup> In order to fully understand these phenomena, the interplay between the nanostructure and the transport properties is required.

In this paper, we present a systematic study of the temperature and frequency dependences of the ac transport properties in granular insulating Co-ZrO<sub>2</sub> thin films, as a function of the Co volume content  $x$ , in the dielectric regime below the Co percolation threshold  $x_p \approx 0.35$ . While the ac conductance can indeed be described *qualitatively* in terms of competing tunneling and capacitance channels, it can also be described *quantitatively* by a random resistor-capacitor cubic network that enables the determination of the microscopic parameters controlling the ac response of the samples. We also show the occurrence, at high temperatures, of a fractional power-law dependence on the frequency of the ac conductance taking place at very low frequencies as compared to the typical ranges at which dispersive behavior is observed in classical-disordered dielectric materials. Besides, the values of the fractional exponent quite less than 0.7 are observed for all Co contents. These values can be easily justified by the semiempirical logarithmic mixing rule for the conductivity of a disordered dielectric material and the effective fraction of tunneling paths deduced for each sample from the comparison between the experimental results and the simulations for a random resistor-capacitor cubic network.

## II. SAMPLES AND STRUCTURAL CHARACTERIZATION

Co-ZrO<sub>2</sub> granular films were grown by KrF laser ablation (wavelength of 248 nm; pulse duration of 34 ns). The samples were deposited at room temperature in a vacuum chamber with rotating composite targets made of sectors of ZrO<sub>2</sub> and pure cobalt. Several surface ratios of target components led to different Co volume fraction  $x$ . About ten samples were prepared in both the dielectric and metallic regimes in the range  $0.13 < x < 0.45$ . The distance between target and substrate was fixed at 30 mm. The laser fluency was typically  $3 \text{ J cm}^{-2}$ .

Average compositions were determined by microprobe analyses. The films were structurally characterized with x-ray diffraction (XRD) and high-resolution transmission electron microscopy (TEM). The substrates for TEM experiments were silicon nitride membrane windows enabling direct observation of as-deposited samples. The particle-size distribution was also obtained by fitting the low-field magnetic susceptibility (zero-field cooling) and high-temperature isothermal magnetization curves  $M(H)$  to a distribution of Langevin functions.<sup>21</sup>

Figure 1 shows bright field TEM images of Co-ZrO<sub>2</sub> thin films for various Co contents. For the sake of simplicity, three samples in the dielectric regime are presented. The dark regions correspond to the Co nanoparticles and light regions to the amorphous ZrO<sub>2</sub> matrix. The particles have very well-defined interfaces with the matrix.<sup>12,20</sup> For Co concentration  $x < 0.31$ , the particles have mostly spherical shape [Figs. 1(a) and 1(b)]; while for  $x \geq 0.31$ , the neighboring particles start to coalesce, giving rise to larger nonspherical particles [Fig. 1(c)], indicating the rapid approach to the percolation threshold.<sup>22</sup> For lower Co content ( $x < 0.22$ ), a bimodal distribution of Co particles is observed (constituted by two log-normal distributions: one centered at smaller sizes; the other at larger ones) since nucleation and growth mechanisms overlap.<sup>20</sup> By increasing the Co content  $x \geq 0.25$ , the bimodal distribution can be no longer distinguished and the histograms of particles sizes can be fitted to an effective, broader, and single log-normal function. For  $x=0.25$ , the mean particle size and the standard deviation are  $D=7.4 \text{ nm}$  and  $\sigma=2.7 \text{ nm}$ , respectively. With further increasing of the metal content  $x=0.30$ , the size distribution shifts to larger sizes ( $D=11 \text{ nm}$ ) with a similar standard deviation ( $\sigma=3.6 \text{ nm}$ ). About  $x=0.35$ , the size distribution broadens abruptly ( $D=15.5 \text{ nm}$  and  $\sigma=7.3 \text{ nm}$ ) because of the massive coalescence of the nanoparticles that leads to percolation.<sup>22</sup>

## III. TRANSPORT PROPERTIES

The ac electrical measurements were carried out by a four-probe technique using a lock-in amplifier and an ac constant source in a frequency range of 10–6000 Hz. Although the digital lock-in amplifier is able to measure signals of very low frequency ( $\sim 1 \text{ Hz}$ ), the measured phase of the impedance is limited to two digits, which gives rise to difficulties in the calculation of imaginary part of the impedance when the phase goes to zero. The films prepared for transport measurements were deposited onto insulating glass substrates with four parallel gold stripes of 1 mm width with a separa-

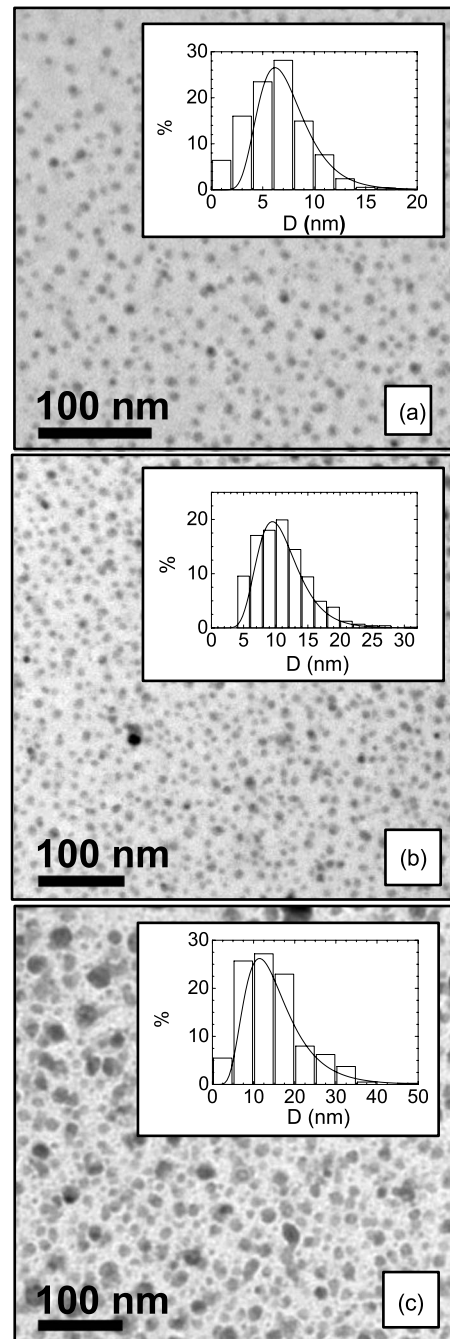


FIG. 1. Bright field TEM images of Co-ZrO<sub>2</sub> films as a function of the Co volume content  $x$ : (a)  $x=0.25$ , (b)  $x=0.30$ , and (c)  $x=0.35$ . In the insets, the histograms of particle sizes obtained after analyzing the TEM micrographs are plotted.

tion of 0.7 mm between the two of them. Measurements were carried out in a closed circuit helium cryostat, varying the sample temperature from 40 K up to room temperature. The dc conductance was extrapolated from measurements at 12 Hz. The temperature dependence of the dc resistivity  $\rho(T)$  in the dielectric regime can be satisfactorily described by thermally assisted tunneling and Coulomb blockade for all samples and follows the expression  $\rho(T) \sim \exp(2\sqrt{B/k_B T})$ ,<sup>4,5,7</sup> where the parameter  $B$  shows strong dependence with Co content (see below).  $B$  is directly related

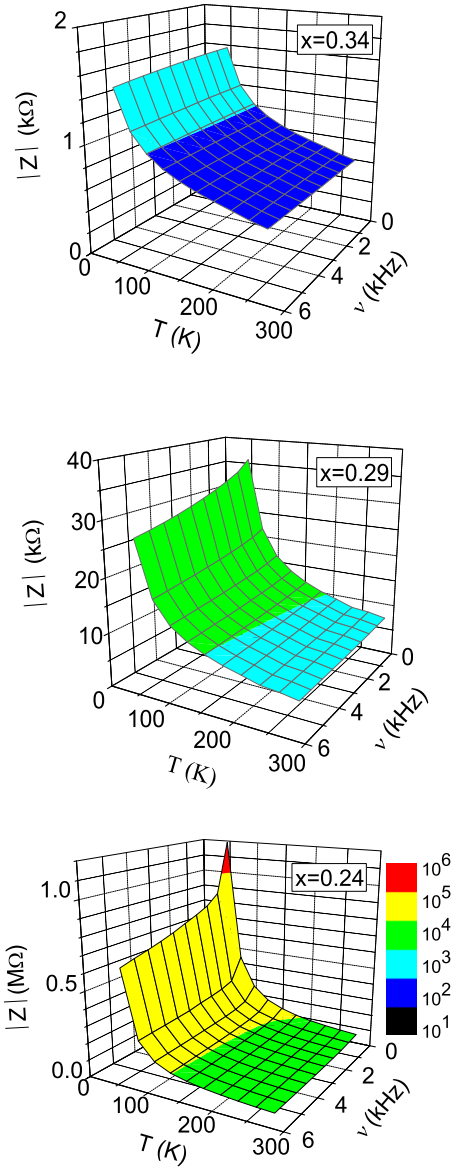


FIG. 2. (Color online) Experimental results for the modulus  $|Z|(\nu, T)$  of the complex impedance for  $x=0.34, 0.29,$  and  $0.24$ .

to the Coulomb charging energy of the particles  $E_C^0$ , as  $B = E_C^0 d\chi$ , being  $d$  the interparticle distance and  $\chi$  as the tunneling barrier height in momentum units.

Figure 2 shows the temperature and frequency dependences of the modulus of the complex impedance  $|Z|$  for  $x = 0.34, 0.29,$  and  $0.24$ . These three samples are taken as representative of the main features of the ac conductance up to the percolation threshold. For all Co contents,  $|Z|$  decreases with increasing temperature in the whole frequency range, since the Coulomb charging energy of the particles is overcome by thermal activation. Moreover,  $|Z|$  decreases with increasing frequency at all temperatures which indicates the existence of capacitive conduction channels in parallel to the tunneling conductance. Finally, the temperature and frequency dependences of  $|Z|$  are more pronounced with decreasing Co content, which is directly related to the decrease in the tunneling probability when particles are further apart, as observed in the zero-frequency limit through the increase

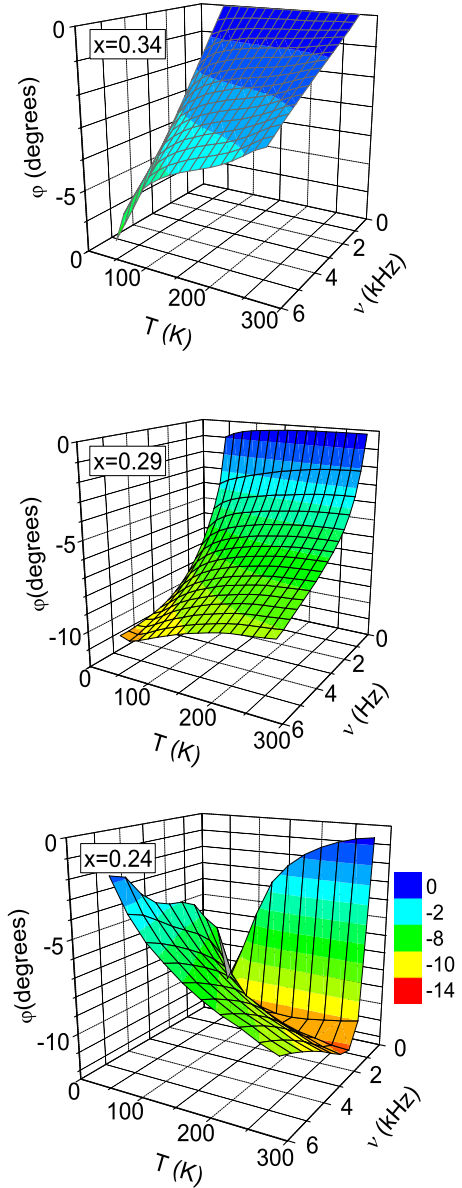


FIG. 3. (Color online) Experimental results for the phase  $\varphi(\nu, T)$  of the complex impedance for  $x=0.34, 0.29,$  and  $0.24$ .

in the parameter  $B$ . As a consequence, the relative contribution of capacitive conductance increases as compared to the tunneling current, resulting in much more pronounced dependence of  $|Z|$  with frequency at low Co content.

Deeper insight in the nature of the electrical paths through the Co particles can be gained by analyzing the frequency and temperature dependences of the phase  $\varphi$  of the complex impedance for various Co concentrations (Fig. 3). At high concentrations ( $x \geq 0.29$ ), high temperatures and frequencies close to the dc limit  $\varphi$  is roughly zero, corresponding to the electron tunneling taking place between metallic Co, which gives rise to an almost pure resistive contribution to the total conductance of the sample. With increasing frequency, high-temperature curves display a decrease in  $\varphi$  as the electron current due to the capacitive effect between particles becomes more and more important as compared to the tunneling current. The decrease in  $\varphi$  is more pronounced at low

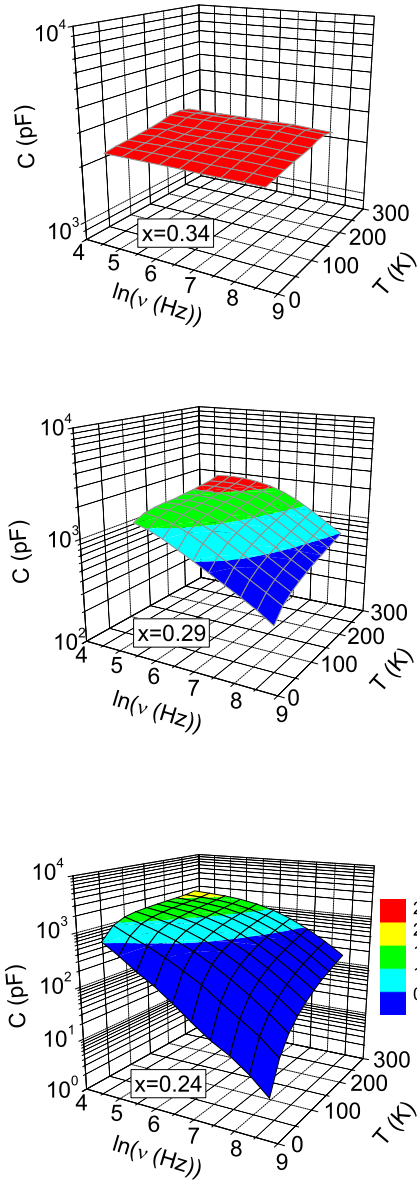


FIG. 4. (Color online) Experimental results of the capacitance for  $x=0.34, 0.29, 0.24$ .

temperatures (electrons cannot be thermally activated to overcome the Coulomb gap so as to tunnel) and it is more significant with the decrease in Co content, as particles are further apart and tunneling conduction becomes ineffective. Then, when the contribution of the conduction through capacitive channels becomes comparable to the tunneling conductivity, one minimum develops in the phase at a frequency which depends both on temperature and Co content  $\nu_{\min}(x, T)$ . This happens at all temperatures for  $x=0.24$  and just at low temperatures for  $x=0.29$ . Finally,  $\varphi$  becomes less negative for frequencies above  $\nu_{\min}(x, T)$  due to the occurrence of shortcuts of capacitive nature between the particles which are further apart (not contributing to direct tunneling), thereby increasing their electrical connectivity and thus contributing to the net tunneling current. With decreasing temperature and Co concentration,  $\nu_{\min}(x, T)$  shifts toward lower frequencies (see  $x=0.24$ ), due to the larger relative contribu-

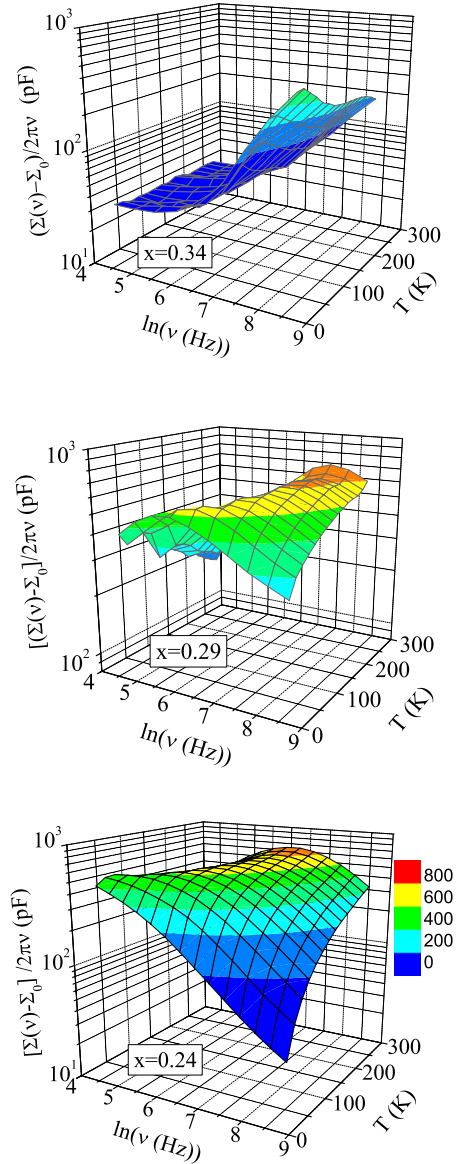


FIG. 5. (Color online) Experimental results for the dielectric loss  $(\Sigma(\omega)-\Sigma_0)/\omega$ , being  $\Sigma$  the conductance, for  $x = 0.34, 0.29, 0.24$ .

tion of those capacitive shortcuts with respect to direct tunneling contributions. For  $x < 0.24$ , the well-defined minimum in  $\varphi$  that it is present at high temperatures broadens and decreases monotonically with frequency as tunneling processes are strongly reduced.<sup>18</sup>

In order to study how the transport properties evolve with the Co content, we analyze the quantities that play the same role that the dielectric constant plays in the case of disordered dielectrics. In our case, the capacitance  $C(\omega)$  (Fig. 4) is proportional to the real part of the dielectric constant, while the so-called dielectric loss—defined as  $[\Sigma(\omega)-\Sigma_0]/\omega$  (Fig. 5), being  $\Sigma$  the conductance—is proportional to the imaginary part of the dielectric constant. In the case of disordered dielectrics, a *universal* response develops when the dielectric loss shows a peak at a certain frequency (dispersive region) and all curves at different temperatures scale onto a single master curve that follows asymptotic power-law behavior

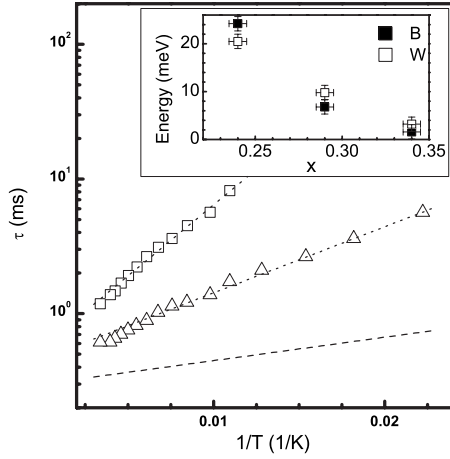


FIG. 6. Relaxation time  $\tau=1/\nu_p$  versus the reciprocal of the temperature, being  $\nu_p$  the frequency of the peak in the dielectric loss, for  $x=0.29$  and  $0.24$ . Dashed lines correspond to the Arrhenius law for samples  $x=0.34$ ,  $0.29$ , and  $0.24$ . The inset shows  $W$  (empty squares) calculated from the Arrhenius law followed by  $\nu_p$ , and  $B$  (full black squares) deduced from the dc resistivity, as functions of the Co content.

with frequency both above and below the frequency of the peak, suggesting the occurrence of an absorption process.<sup>13</sup> This *universal* response may correspond to a Debye-type process when the frequency of the peak of the dielectric loss follows a thermal-activated dependence with temperature<sup>13</sup> as is the case of the systems studied in this work. However, in granular insulating thin films, the absorption phenomenon is related to the existence of competing thermally activated tunneling and capacitive paths rather than being due to the occurrence of a true Debye-type-activated relaxation process.<sup>23</sup>

The dielectric loss (Fig. 5) increases significantly as a function of frequency when the Co concentration approaches the percolation threshold (low-temperature range for  $x=0.34$ ) and develops a peak at  $\nu_p(x, T)$  in the intermediate range of Co content  $0.24 \leq x < 0.34$ . The peak position  $\nu_p(x, T)$  shifts toward lower frequencies with decreasing temperature and Co content (as conductance through capacitance dominates) and finally disappears below the lowest measuring frequency available in our experimental setup (10 Hz) in the low-temperature range for  $x=0.24$ . At the same time, the capacitance also follows a power-law behavior (note the double-logarithmic scale in Fig. 5) that shifts toward smaller frequencies as temperature and Co content decrease.

The thermal dependence of the characteristic relaxation time at the loss peak, which is defined as  $\tau(x, T) = 1/\nu_p(x, T)$  (Fig. 6), is found to follow an Arrhenius law,<sup>11,12</sup>  $\tau(x, T) = \tau_0 \exp(W/k_B T)$ , being the value of the activation energy  $W$  comparable to that of the parameter  $B$  in the temperature dependence of the dc resistivity for the three sample studied in this work (see the inset to Fig. 6). As  $B$  gives the energy scale of the thermally activated tunneling processes in the Coulomb blockade regime, while the maximum of the dielectric-loss peak takes place when tunneling and capacitive admittances are comparable, it is reasonable to expect that  $B$  and  $W$  will be comparable, since  $W$  gives the energy

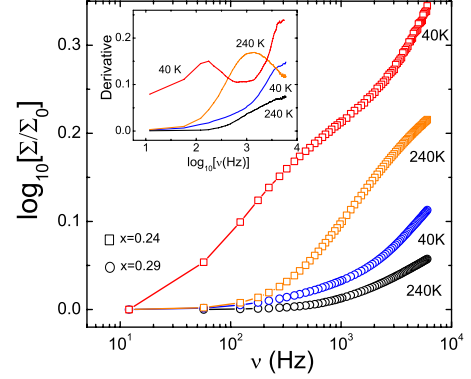


FIG. 7. (Color online)  $\log_{10}$ - $\log_{10}$  plot of the conductance normalized with respect to the dc value as a function of the frequency at constant temperatures which are indicated at the right side of each curve. Empty squares and circles correspond to  $x=0.24$  and  $x=0.29$ , respectively.  $\Sigma_0$  represents the conductance in the dc limit. The inset shows the derivatives of  $\log_{10}[\Sigma/\Sigma_0]$  with respect to  $\log_{10}[\nu(\text{Hz})]$ . The curves correspond to  $x=0.24$  and  $x=0.29$  from top to bottom and the temperature is indicated close to each curve.

scale associated with the dielectric-loss peak. Moreover, using  $W$  as a scaling parameter, the dielectric loss and capacitance at different temperatures collapse onto a single master curves when they are represented as a function of the scaling variable  $\nu \exp(W/k_B T)$  (Refs. 11 and 12) (not shown). We note that for the case  $x=0.34$ , the dashed line in Fig. 6 corresponds to the Arrhenius law for the value of  $W$  deduced from the scaling of the dielectric loss and capacitance since these two quantities do not show any peak in the studied range of frequencies as shown in Fig. 5. Summarizing, the shift of the dielectric loss and capacitance toward lower frequencies with decreasing temperature and Co content is mainly caused by the decrease in the density of charge carriers (see the inset to Fig. 6).

Moreover, the dispersive behavior of these granular materials yields a fractional power-law dependence of the conductance on the frequency, as is expected for any system which is a complex random network composed of resistive and capacitive paths.<sup>17</sup> Figure 7 shows the  $\log_{10}$ - $\log_{10}$  plot of the conductance normalized to the corresponding dc value as a function of the frequency at 40 and 240 K for  $x=0.24$  and  $x=0.29$ , which are values of the temperature and Co content yielding representative cases. For all the curves, we observe a low-frequency plateau, where the dc conductance dominates, and a dispersive region taking place in the frequency range within which the magnitudes of the admittances of the tunneling and capacitive paths become similar. Consequently, the onset of the dispersive region is located at lower frequencies as the tunneling conductivity is reduced by the decreasing of either the temperature or Co content (the tunneling conductance of the samples shows a much stronger dependence on Co content than the capacitance because of the exponential dependence of the tunneling probability on the interparticle distance). The inset to Fig. 7 shows that the slope of  $\log_{10}[\Sigma/\Sigma_0]$  versus  $\log_{10}[\nu]$  is a function of frequency, as previously reported for a random resistor-capacitor (R-C) network,<sup>19</sup> indicating the occurrence of a fractional power-law behavior with a frequency-dependent exponent.

The maximum values of this exponent at  $T=240$  K are 0.17 for  $x=0.24$  and 0.07 for  $x=0.29$ ; the overall shape of the slope curves being quite similar to that of a R-C network<sup>19</sup> composed of a random distribution of resistive and capacitive electrical bonds. This can be understood taking into account the thermally assisted nature of the tunneling conduction between particles that yields a contribution to the admittance at 240 K high enough as to be comparable—at intermediate frequencies—to that of the capacitance between larger particles, which are far apart (not contributing to direct tunneling), but very much higher than the admittance associated with the capacitance between tunneling particles, which can be neglected. Accordingly, at high temperatures the electrical backbone of the system can be well described by a random distribution of capacitive and resistive paths like in the R-C network model, for which the conductance can be approximated from the logarithmic mixing rule<sup>24</sup> to be proportional to  $\nu^{1-x_r}$ , within the frequency range for which the contributions to the admittance of the capacitive and resistive paths are similar. Since  $x_r$  is the fraction of electrical bonds occupied by resistors in the R-C model, we can estimate the fraction of tunneling paths in the samples from the maximum values of the slope curves in the inset to Fig. 7 to be 0.83 and 0.93 for  $x=0.24$  and  $x=0.29$ , respectively.

At low temperatures, the density of charge carriers is strongly reduced by the effect of the Coulomb gap; a fact which decreases correspondingly the contribution of the tunneling processes to the net admittance of the sample. Therefore, the onset of the dispersive region shifts toward zero as the admittances of both tunneling and capacitive channels become similar at lower frequencies. This is clearly shown by the curve at 40 K for  $x=0.24$  in Fig. 7 which below at about  $7 \times 10^2$  Hz essentially follows the shape of that at 240 K but shifted to lower frequencies as is shown by the corresponding slope curves in the inset to Fig. 7. Above at about  $7 \times 10^2$  Hz an abrupt upward turn round of  $\log_{10}[\Sigma/\Sigma_0]$  is observed which indicates the onset of a second dispersive region associated with the contribution of the capacitance between smaller particles shortcircuiting tunneling channels. Consequently, as the frequency is further increased, the effective fraction of resistive paths (tunneling paths) is reduced increasing the slope of  $\log_{10}[\Sigma/\Sigma_0]$  versus  $\log_{10}[\nu]$  (see curve at 40 K for  $x=0.24$  in the inset to Fig. 7). A similar behavior is displayed by the curve at 40 K for  $x=0.29$  with respect to that at 240 K but with more rounded features and the two dispersive regions not being so clearly differentiated because of the broadening of the particle-size distribution as the Co content increases.

#### IV. RANDOM R-C NETWORK

All the foregoing can be successfully modeled by a random R-C network<sup>23,25</sup> reproducing the conductance among particles. The network consists of a cubic arrangement of 2900 electrical bonds connecting the nodes of the lattice. Each node symbolizes a particle and is connected to its six-nearest neighbors through an electrical bond, except for the nodes at the edges and corners, which have reduced connec-

tivity. The nodes at the left-hand side of the network are all connected to the first node, which plays the role of a flat electrode. The same holds for the nodes at the right-hand side of the network, which are all connected to the last node. An ac current source is connected between the first and last nodes, and the amplitude and the phase of the voltage drop through the network are calculated as a function of frequency using the circuit simulation software WINSPIICE.<sup>26</sup> A fraction  $x_r$  of the electrical bonds chosen at random is occupied by a parallel combination of a resistance  $R_t$  and a capacitance  $C_p$ , and the rest  $(1-x_r)$  is occupied by a capacitance  $C'_p$ .  $R_t$  and  $C_p$  represent, respectively, the tunneling resistance and capacitance between small particles which are close together, while  $C'_p$  represents the capacitance of the large particles that are further apart.  $C'_p$  is much larger than  $C_p$  since the capacitance between two facing particles of similar size is roughly proportional to the particle size. The tunneling between larger particles further apart is neglected due to the exponential increase in the effective resistance associated with tunneling processes with interparticle distance. As already pointed out by Abeles *et al.*,<sup>4</sup> electrons tunnel between particles of approximately the same size, i.e., cannot tunnel either to a smaller particles—since the Coulomb charging energy is larger—or to a larger particles which are further apart.

From the average distances and sizes in Fig. 1 and using the analytical expression for the capacitance between two equal metallic particles proposed by Roy,<sup>27</sup> we estimated the following values:  $C'_p=8.8 \times 10^{-19}$  F for  $x=0.24$  (7 nm particles with an average separation of 6 nm);  $C'_p=1.4 \times 10^{-18}$  F for  $x=0.29$  (11 nm particles with an average separation of 9 nm); and  $C'_p=3.5 \times 10^{-18}$  F for  $x=0.34$  (15 nm particles with an average separation of 7 nm). Assuming that  $C'_p$  is temperature independent, an estimation of the rest of the parameters ( $x_r$ ,  $R_t$ , and  $C_p$ ) as a function of the temperature is obtained by fitting experimental data for  $\varphi(\nu, T)$  in Fig. 3 to the response of the random R-C network. The calculated  $\varphi(\nu, T)$  surfaces obtained for the R-C model are shown in Fig. 8.

First, it is worth noting that  $\varphi(\nu, T)$  surfaces for all three Co contents obtained from the R-C model in Fig. 8 are identical to the experimental ones in Fig. 3, which strongly supports our basic assumption that the ac conductance of granular insulating thin films can be well accounted for by the competition of randomly distributed tunneling and capacitive paths. Second, the resistive fraction  $x_r$  is almost temperature independent and increases with Co content indicating increasing conduction through tunneling channels, as expected. The fitted values are the following:  $x_r=0.89$  for  $x=0.24$ ,  $x_r=0.95$  for  $x=0.29$ , and  $x_r=0.97$  for  $x=0.34$ . It is remarkable that the fitted values of  $x_r$  for  $x=0.24$  and  $x=0.29$  are in good agreement with those deduced from the dispersive region of the experimental conductance at 240 K (see Fig. 7).

The temperature dependence of  $R_t$  is shown in Fig. 9. The average tunneling resistance between neighboring particles evaluated from the model is in, qualitatively, agreement with the experimental dc resistance of the samples multiplying it by an arbitrary scale factor (Fig. 9), showing the expected behavior for thermally assisted tunneling in the dielectric regime.<sup>4,5,7,11,12</sup> In contrast,  $C_p$  is almost temperature inde-

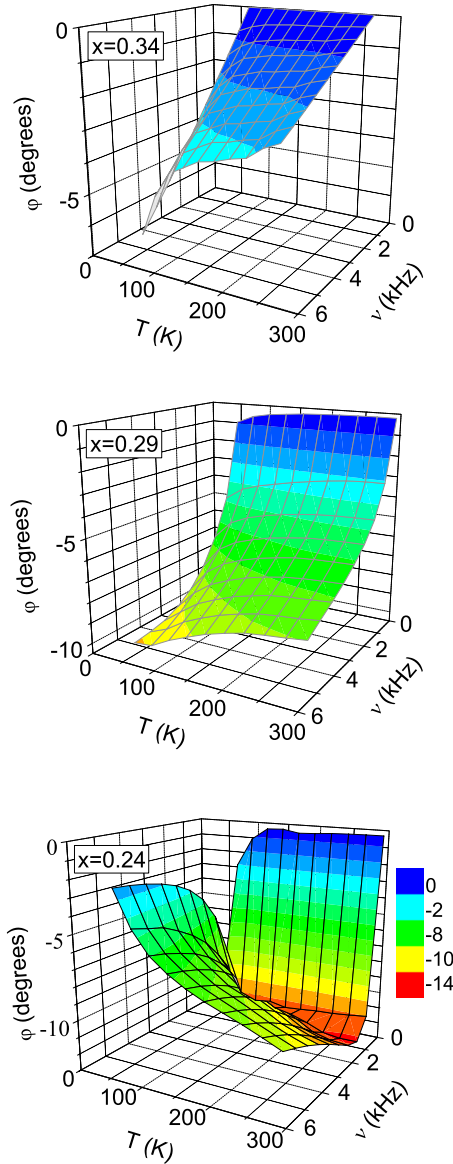


FIG. 8. (Color online) Results from the random R-C network for the phase  $\varphi(\nu, T)$  of the complex impedance for  $x = 0.34, 0.29, 0.24$  (see Sec. IV).

pendent, as expected, and increases with Co content, thus approaching  $C_p'$  as conduction paths are formed when percolation threshold is reached. The calculated values are  $C_p = 10^{-21}$  F for  $x=0.24$ ;  $C_p = 1.5 \times 10^{-20}$  F for  $x=0.29$ ; and  $C_p = 3 \times 10^{-19}$  F for  $x=0.34$ .

## V. CONCLUSIONS

In conclusion, the temperature and frequency dependences of the ac transport properties in granular Co-ZrO<sub>2</sub> thin films for several Co contents have been analyzed in detail. The so-called *universal* behavior is observed below the percolation threshold in the range of Co concentration  $0.24 \leq x < 0.34$ . The ac response is a direct consequence of the competition between two kinds of parallel channels of conduction; one by thermally activated tunneling through

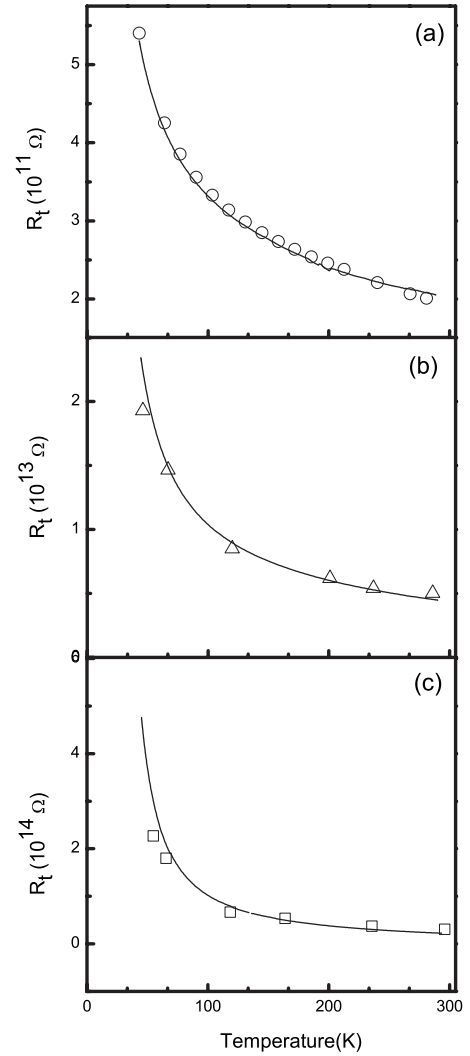


FIG. 9. Temperature dependence of the total dc resistance of the samples (solid lines) as compared to  $R_t(T)$  obtained from the fit of  $\varphi(\nu, T)$  to a random R-C network (empty symbols), for (a)  $x = 0.34$ , (b) 0.29, and (c) 0.24. The total dc resistance data have been multiplied by arbitrary constants to achieve superimposition with  $R_t(T)$  data.

small particles of approximately the same size and a second one through capacitive conduction between particles. This is in agreement with the underlying nanostructure observed by high-resolution transmission electron microscopy. A random R-C network of resistors and capacitors reproduces very well the overall experimental ac behavior in the whole range of  $\nu$  and  $T$ , for all metal content. Finally, it is worth noting that the ac conductance shows fractional power-law dependences on the frequency, taking place at very low frequencies as compared to the typical ranges at which dispersive behavior is observed in disordered dielectric materials. In fact, two dispersive regions are observed at low temperatures. The first one is associated with the competition between tunneling channels and capacitive ones among large particles, which are further apart so as not contributing to the tunneling processes. The second dispersive region is associated with the additional contribution of the capacitance between smaller particles shortcutting tunneling channels. At high tempera-

tures, the second dispersive region is not observed because it is out of the experimental frequency range. The values of the fractional exponent for the first dispersive region, which are quite less than 0.7, are in good agreement with the fraction of tunneling paths deduced from the fitting of the experimental phase of the complex impedance to the R-C network model.

#### ACKNOWLEDGMENTS

M. Varela (University of Barcelona) is acknowledged for

his support during the sample preparation. We would also like to thank the staff of the Scientific and Technical facilities of the University of Barcelona. Financial support of the Spanish CICYT (Grant No. MAT2006-03999) and Catalan DURSI (Grant No. 2005SGR00969) are gratefully recognized. Z.K. thanks Spanish MEC for the financial support through Juan de la Cierva and Ramón y Cajal programs. M.K. thanks the Spanish MEC for financial support.

- 
- <sup>1</sup>X. Batlle and A. Labarta, *J. Phys. D* **35**, R15 (2002).  
<sup>2</sup>C. L. Chien, *Science and Technology of Nanostructured Magnetic Materials*, edited by G. C. Hadjipanayis and G. A. Prinz (Plenum, New York, 1991), p 477.  
<sup>3</sup>C. L. Chien, *J. Appl. Phys.* **69**, 5267 (1991).  
<sup>4</sup>B. Abeles, P. Sheng, M. D. Coutts, and Y. Arie, *Adv. Phys.* **24**, 407 (1975).  
<sup>5</sup>B. Abeles, in *Applied Solid State Science: Advances in Materials and Device Research*, edited by R. Wolfe (Academic, New York, 1976).  
<sup>6</sup>C. L. Chien, J. Q. Xiao, and J. S. Jiang, *J. Appl. Phys.* **73**, 5309 (1993).  
<sup>7</sup>P. Sheng, B. Abeles, and Y. Arie, *Phys. Rev. Lett.* **31**, 44 (1973).  
<sup>8</sup>H. Fujimori, S. Mitani, and S. Ohnuma, *J. Magn. Magn. Mater.* **156**, 311 (1996).  
<sup>9</sup>A. Milner, A. Gerber, B. Groisman, M. Karpovsky, and A. Gladkikh, *Phys. Rev. Lett.* **76**, 475 (1996).  
<sup>10</sup>M. Holdenried and M. Micklitz, *Eur. Phys. J. B* **13**, 205 (2000).  
<sup>11</sup>B. J. Hattink, A. Labarta, M. García del Muro, X. Batlle, F. Sánchez, and M. Varela, *Phys. Rev. B* **67**, 033402 (2003).  
<sup>12</sup>B. J. Hattink, M. García del Muro, Z. Konstantinović, V. F. Puentes, X. Batlle, and A. Labarta, *Int. J. Nanotechnol.* **2**, 43 (2005).  
<sup>13</sup>A. K. Jonscher, *Nature (London)* **267**, 673 (1977); *J. Phys. D* **32**, R57 (1999).  
<sup>14</sup>J. C. Dyre and T. B. Schroder, *Rev. Mod. Phys.* **72**, 873 (2000).  
<sup>15</sup>A. G. Hunt, *Philos. Mag. B* **81**, 875 (2001).  
<sup>16</sup>E. Tuncer, Y. W. Serdyuk, and S. M. Gubanski, *IEEE Trans. Dielectr. Electr. Insul.* **9**, 809 (2002).  
<sup>17</sup>D. P. Almond and C. R. Bowen, *Phys. Rev. Lett.* **92**, 157601 (2004).  
<sup>18</sup>T. B. Schrøder and J. C. Dyre, *Phys. Rev. Lett.* **84**, 310 (2000).  
<sup>19</sup>A. N. Papathanassiou, I. Sakellis, and J. Grammatikakis, *Appl. Phys. Lett.* **91**, 122911 (2007).  
<sup>20</sup>Z. Konstantinović, M. García del Muro, M. Varela, X. Batlle, and A. Labarta, *Appl. Phys. Lett.* **91**, 052108 (2007).  
<sup>21</sup>B. J. Hattink, M. García del Muro, Z. Konstantinović, X. Batlle, A. Labarta, and M. Varela, *Phys. Rev. B* **73**, 045418 (2006).  
<sup>22</sup>Z. Konstantinović, M. García del Muro, X. Batlle, A. Labarta, and M. Varela, *Nanotechnology* **17**, 4106 (2006).  
<sup>23</sup>B. Vainas, D. P. Almond, J. Luo, and R. Stevens, *Solid State Ionics* **126**, 65 (1999).  
<sup>24</sup>K. Lichtenecker, *Phys. Z.* **28**, 417 (1927).  
<sup>25</sup>J. C. Dyre, *Phys. Rev. B* **48**, 12511 (1993).  
<sup>26</sup>WINSPIICE by M. Smith based on Spice 3F4 which was developed by the Department of Electrical Engineering and Computer Science at the University of Berkeley, <http://www.willingham2.freemove.co.uk/winspice.html>  
<sup>27</sup>S. A. Roy, "Simulation tools for the analysis of single electronic systems," Ph.D. thesis, University of Glasgow, 1994.